

Globally optimized finite-difference extrapolator for strongly VTI media

Jin-Hai Zhang¹ and Zhen-Xing Yao¹

ABSTRACT

Implicit finite-difference (FD) migration is unconditionally stable and is popular in handling strong velocity variations, but its extension to strongly transversely anisotropic media with vertical symmetric axis media is difficult. Traditional local optimizations generate the optimized coefficients for each pair of Thomsen anisotropy parameters independently, which can degrade results substantially for large anisotropy variations and lead to a huge table. We developed an implicit FD method using the analytic Taylor-series expansion and used a global optimization scheme to improve its accuracy for wide phase angles. We first extended the number of the constant coefficients; then we relaxed the coefficient of the time-delay extrapolation term by tuning a small factor such that error is less than 0.1%. Finally, we optimized the constant coefficients using a simulated annealing algorithm by constraining that all the error functions on a

fine grid of the whole anisotropic region did not exceed 0.5% simultaneously. The extended number of the constant coefficients and the relaxed coefficient greatly enhanced the flexibility of matching the dispersion relation and significantly improved the ability of handling strong anisotropy over a much wider range. Compared with traditional local optimization, our scheme does not need any table and table lookup. For each order of the FD method, only one group of optimized coefficients is enough to handle strong variations in velocity and anisotropy. More importantly, our global optimization scheme guarantees the accuracy for various possible ranges of anisotropy parameters, no matter how strong the anisotropy is. For the globally optimized second-order FD method, the accurate phase angle is up to 58°, and the increase is about 18°–22°. For the globally optimized fourth-order FD method, the accurate phase angle is up to 77°, and the increase is about 22°–27°.

INTRODUCTION

It is now well recognized that seismic anisotropy widely exists in the earth. Large positioning errors or a complete loss of substructures may be caused if seismic anisotropy is not well considered during seismic migration (Larner and Cohen, 1993; Etgen et al., 2009). Many wave-equation depth-migration methods have been extended from traditional isotropic cases, such as the one-way method and the two-way method (i.e., reverse time migration). Extension of the two-way method is very simple because only direct discretization on the anisotropic wave equation is sufficient (Zhang and Zhang, 2009). The drawback of the two-way method is the huge memory demand and computational cost, especially for large-scale 3D cases. In contrast, the one-way method is much more attractive in memory demand and computational cost because a 3D problem is approximated as many cascaded 2D problems along the depth direction (Claerbout, 1985). However, unlike with isotropic media,

the one-way propagator design is fairly difficult because the dispersion relation for anisotropic media is much more complex even for the simplest anisotropy case, the transversely anisotropic media with vertical symmetric axis (VTI) media. As a reasonable approximation to the general anisotropic media, the VTI media are very popular for imaging complex substructures.

For laterally homogeneous VTI media, the phase-shift method (Meadows and Abriel, 1994), the simplest Fourier method, is accurate up to 90°. For laterally heterogeneous VTI media, high-order expansions are usually needed for the Fourier method to handle steep dips as well as the impact of anisotropic effects (Le Rousseau, 1997; Le Rousseau and de Hoop, 2001; Ferguson and Margrave, 2002). Unfortunately, the accurate dip angle of the Fourier method is very limited in the presence of strong velocity contrasts even for the isotropic cases. Explicit operators are famous in handling strong velocity contrasts (Uzcategui, 1995; Zhang et al., 2001; Thorbecke et al., 2004; Ren et al., 2005), but they may have potential stability

Manuscript received by the Editor 13 December 2011; revised manuscript received 22 February 2012; published online 18 June 2012.

¹Chinese Academy of Sciences, Institute of Geology and Geophysics, Beijing, China. E-mail: zjh@mail.iggcas.ac.cn; yaozx@mail.iggcas.ac.cn.
© 2012 Society of Exploration Geophysicists. All rights reserved.

problems (Etgen, 1994). In contrast, implicit finite-difference (FD) methods are attractive because of their unconditional stability (Claerbout, 1985); thus, they can be safely used in imaging complex media with wide-angle structures. Furthermore, the implicit FD methods are good at handling strong velocity variations. Therefore, implicit FD methods received increased attention recently in imaging VTI media, either as independent methods or as high-order corrections to the phase-shift method (Ristow, 1999; Han and Wu, 2005; Zhang et al., 2005b; Hua et al., 2006; Fei and Liner,

2008; Bakker, 2009; Shan, 2009; Zhang, 2009; Amazonas et al., 2010; Pedersen et al., 2010).

In seismic migration, we usually limit the number of terms to keep the computational efficiency and turn to optimization methods to improve the numerical accuracy (Lee and Suh, 1985; Xie and Wu, 1999; Huang and Fehler, 2000; Zhu et al., 2008; Shan, 2009). The optimization methods usually only change the constant coefficients of the traditional expansions by matching the expanded operator to the dispersion relation; thus, without changing the expansion order and the algorithmic structure, the accuracy can be significantly improved after using optimization. The optimization schemes of seismic migration can be categorized into two classes: the local optimization scheme and the global optimization scheme. The local optimization scheme is table-driven and has very high accuracy because it is tailor-made for a given model (e.g., Ristow and Rühl, 1994; Liu and Zhang, 2006; Shan, 2009). In contrast, the global optimization scheme is independent of tables and is suitable for all possible models (e.g., Lee and Suh, 1985; Xie and Wu, 1999; Huang and Fehler, 2000; Zhu et al., 2008; Zhang et al., 2010; Zhang and Yao, 2011).

Ristow (1999) designs an implicit FD scheme using the analytic Taylor-series expansion under the assumption of weak anisotropy. He also suggests a local optimization scheme, but the resulting accuracy is only 70° for the sixth-order FD method. For strong anisotropy, Shan (2009) designs a second-order implicit FD scheme by the analytic Taylor-series expansion and estimates a simplified form of the fourth-order FD method. Shan's optimized FD method is accurate to 60° for the second-order operator and to 80° for the fourth-order operator, which is more accurate than the method devised by Ristow (1999). Based on the local optimization scheme, their optimized coefficients are functions of Thomsen anisotropy parameters (Thomsen, 1986), which can be calculated before wavefield extrapolation and stored in a table.

Theoretically, each group of the locally optimized coefficients is only valid for the pair of Thomsen anisotropy parameters that are used to obtain the optimized coefficients. In other words, the optimized coefficients based on a pair of Thomsen anisotropy parameters are potentially harmful to other Thomsen anisotropy parameters, even to the immediate neighboring parameters (see Figure 1 for details). Consequently, it is not perfectly safe to use these independently optimized coefficients for imaging steep dips in the presence of strong variations in velocities and anisotropy parameters, even though we could have observed high accuracy by examining their dispersion relations. Although it is not impossible to produce a more reliable table by a much denser grid over a given anisotropic region, the computational cost of generating the table and of the table lookup would encounter great challenge, because the number of the grid nodes over a strongly anisotropic region is probably up to several million. Therefore, we should guarantee that the optimized coefficients are suitable for all possible distributions of the Thomsen anisotropy parameters, at least for most practical cases.

In this paper, we first present an implicit FD method for a VTI medium by the analytic Taylor-series expansion. Then, we propose a new global optimization scheme to ascertain that the optimized constant coefficients of the implicit FD method are suitable for arbitrary Thomsen anisotropy parameters. The optimized coefficients are obtained by the simulated annealing algorithm (Kirkpatrick et al., 1983; Sen and Stoffa, 1991), a more powerful tool compared

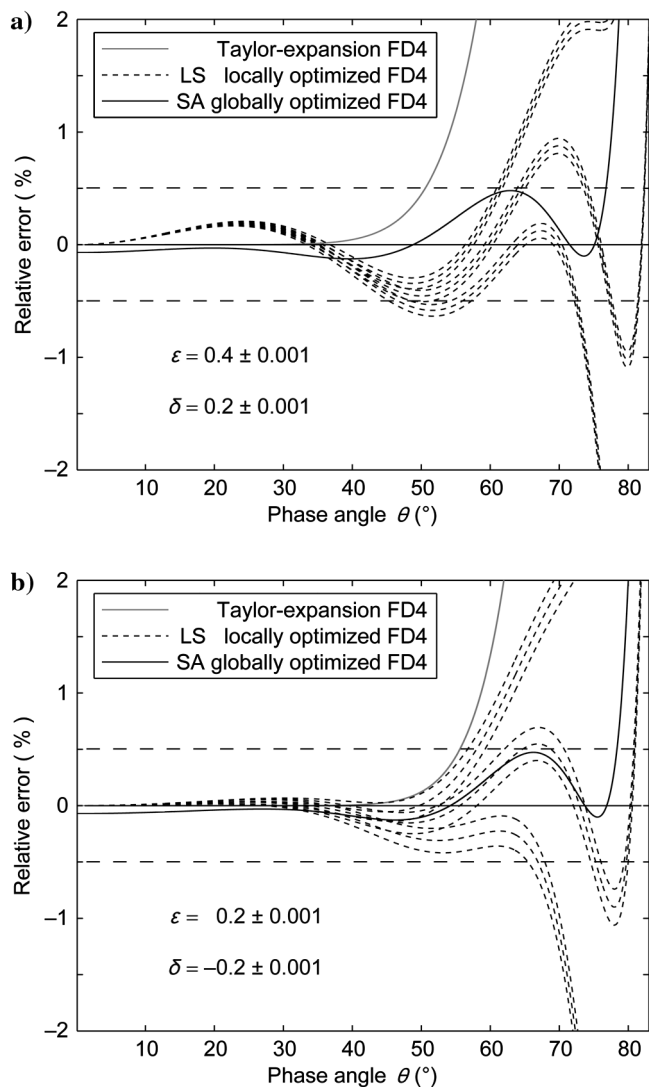


Figure 1. Comparison among three fourth-order FD methods: (a) the central anisotropy parameters are $\epsilon = 0.4$ and $\delta = 0.2$, (b) the central anisotropy parameters are $\epsilon = 0.2$ and $\delta = -0.2$. The nearest nine points around the central anisotropy parameters, with a uniform interval of 0.001, are selected to check the accuracy and robustness of the FD methods. Three possible values of ϵ are $\epsilon - 0.001$, ϵ and $\epsilon + 0.001$; similarly, three possible values of δ are $\delta - 0.001$, δ and $\delta + 0.001$. In each subfigure, gray curves are generated by the FD method using the analytic Taylor-series expansion (i.e., equation 4), dashed curves are generated by the locally optimized FD method using the least-squares approach (i.e., equation 13 in the text and Table 2 in Shan, 2009), and solid curves are generated by the globally optimized FD method using the simulated annealing algorithm (i.e., equation 12).

with the generally used least-squares approach, on a fine grid over a wide range of Thomsen anisotropy parameters. As a global optimization scheme, our scheme only outputs a unique group of optimized coefficients for each order of the implicit FD method. Although we also obtain the optimized coefficients by matching the VTI dispersion relation as in [Shan \(2009\)](#), our optimized coefficients are perfectly safe to each pair of possible Thomsen anisotropy parameters within any practical range, no matter whether for weak, strong, extreme cases, or for any subregion. Our globally optimized coefficients enable the second-order FD method to be accurate up to 58° ; whereas the unoptimized method is only accurate to about 36° . For the fourth-order FD method, using our globally optimized coefficients, the accuracy in phase angle is up to 77° as opposed to an accuracy of 53° for the unoptimized method.

FD SCHEME USING TAYLOR-SERIES EXPANSION

The downward extrapolation wave equation for 2D VTI media in the frequency domain is given by ([Alkhalifah, 1998, 2000](#); [Shan, 2009](#))

$$\frac{\partial P}{\partial z} = ik_z P, \quad (1)$$

with the vertical wavenumber k_z defined as

$$k_z = \frac{\omega}{v} \sqrt{1 - \frac{(1 + 2\delta)u^2}{1 - 2(\varepsilon - \delta)u^2}}, \quad (2)$$

where $v \equiv v(x, z)$ is the phase velocity of the q P-wave in the vertical direction, ε and δ are Thomsen anisotropy parameters ([Thomsen, 1986](#)), $u^2 \equiv v^2 k_x^2 / \omega^2$, ω is the circular frequency, $i = \sqrt{-1}$ is the imaginary unit, and $P \equiv P(x, z; \omega)$ is the wavefield in the frequency domain. The vertical wavenumber k_z can be expanded in an N th-order Taylor series as follows:

$$k_z \approx \frac{\omega}{v} \sum_{n=0}^N t_n u^{2n}, \quad (3)$$

with the first five coefficients being

$$\begin{aligned} t_0 &= 1, & t_1 &= -\frac{1}{2}\lambda, & t_2 &= -\frac{1}{8}(\lambda^2 + 4\lambda\eta), \\ t_3 &= -\frac{1}{16}(\lambda^3 + 4\lambda^2\eta + 8\lambda\eta^2), \\ t_4 &= -\frac{1}{128}(5\lambda^4 + 24\lambda^3\eta + 48\lambda^2\eta^2 + 64\lambda\eta^3), \end{aligned} \quad (4)$$

where $\lambda \equiv (1 + 2\delta)$ and $\eta \equiv 2(\varepsilon - \delta)$.

Equation 3 corresponds to a high-order FD scheme that is extremely difficult to handle, thus, we should limit the highest order of u to be two using the following cascaded form ([Ma, 1982](#); [Claerbout, 1985](#))

$$k_z \approx \bar{k}_z = \frac{\omega}{v} \left(1 - \frac{\alpha_1 u^2}{1 - \beta_1 u^2} - \frac{\alpha_2 u^2}{1 - \beta_2 u^2} - \dots \right). \quad (5)$$

Using the method of indeterminate coefficients ([Ma, 1982](#); [Ristow and Rühl, 1994](#); [Fei and Liner, 2008](#)), we can represent

the coefficients of equation 5 (i.e., $\alpha_1, \beta_1, \alpha_2, \beta_2, \dots$) using $t_1 \sim t_N$. For the second-order FD method (i.e., $N = 2$), $\alpha_1 = 0.5\lambda$ and $\beta_1 = 0.25\lambda + \eta$. For the fourth-order FD method (i.e., $N = 4$), $\alpha_1 = 0.361803340\lambda$, $\beta_1 = 3.05572809\lambda + \eta$, $\alpha_2 = 0.13819660\lambda$, and $\beta_2 = 2.61803399\lambda + \eta$.

According to the relation $\partial^2/\partial x^2 \Leftrightarrow -k_x^2$, the fourth-order FD scheme can be decomposed into three cascaded equations

$$\frac{\partial P}{\partial z} = \frac{i\omega}{v} P, \quad (6)$$

$$\frac{\partial P}{\partial z} = \frac{i\alpha_1 \frac{v}{\omega} \frac{\partial^2}{\partial x^2}}{1 + \beta_1 \frac{v^2}{\omega^2} \frac{\partial^2}{\partial x^2}} P, \quad (7)$$

and

$$\frac{\partial P}{\partial z} = \frac{i\alpha_2 \frac{v}{\omega} \frac{\partial^2}{\partial x^2}}{1 + \beta_2 \frac{v^2}{\omega^2} \frac{\partial^2}{\partial x^2}} P. \quad (8)$$

The second-order FD scheme only includes equations 6 and 7.

GLOBAL OPTIMIZATION SCHEME

We can optimize the constant coefficients of equation 5 to improve the accuracy without any other changes to the implementation of the FD method. We construct an objective function of the fourth-order FD method as

$$E \equiv \left| \frac{\bar{k}_z - k_z}{k_z} \right|. \quad (9)$$

The wavenumber and phase angle are linked by ([Shan, 2009](#))

$$\sin^2 \theta = \frac{V^2(\theta) k_x^2}{\omega^2}, \quad (10)$$

with

$$\begin{aligned} \frac{V^2(\theta)}{v^2} &= \frac{1}{2} + \varepsilon \sin^2 \theta \\ &+ \frac{1}{2} \sqrt{(1 + 2\varepsilon \sin^2 \theta)^2 - 2(\varepsilon - \delta) \sin^2 2\theta}, \end{aligned} \quad (11)$$

where θ is the phase angle away from the vertical direction, $V(\theta)$ is the q P-wave phase velocity in acoustic VTI media and v is the phase velocity in the vertical direction ([Tsvankin, 1996](#); [Alkhalifah, 1998, 2000](#)). Recalling $u^2 \equiv v^2 k_x^2 / \omega^2$, we obtain

$$u^2 = \frac{v^2 \sin^2 \theta}{V^2(\theta)}. \quad (12)$$

Therefore, we can represent the objective function (i.e., equation 9) in terms of only phase angle θ as well as Thomsen anisotropy parameters ε and δ .

In this paper, we present a group of robust optimized coefficients for all pairs of ε and δ within a wide range, so that we can handle strong anisotropy and strong anisotropy variations. We limit the ranges of the Thomsen anisotropy parameters as $\varepsilon \in [\varepsilon_{\min}, \varepsilon_{\max}]$

and $\delta \in [\delta_{\min}, \delta_{\max}]$; thus, we can find some group of optimized coefficients within an angle range of $\theta \in [0^\circ, \theta_{\max}]$ under a given error threshold T (e.g., 1% or 0.5%). If this group of optimized coefficients is suitable for all pairs of ϵ and δ on a fine grid of $\epsilon \in [\epsilon_{\min}, \epsilon_{\max}]$ and $\delta \in [\delta_{\min}, \delta_{\max}]$, we assume that this group of optimized coefficients is suitable for the entire range of $\epsilon \in [\epsilon_{\min}, \epsilon_{\max}]$ and $\delta \in [\delta_{\min}, \delta_{\max}]$. In other words, we first set a grid to cover a given region of Thomsen anisotropy parameters, then we try to find a group of optimized coefficients that satisfies $E(\theta, \epsilon, \delta) \leq T$ on all grid nodes simultaneously. Next, our task is to find such a group of optimized coefficients to maximize θ_{\max} .

The basic idea of coefficient optimization is to match the approximated dispersion relation \bar{k}_z (equation 5) with the true dispersion relation k_z (equation 2) within a wider angle range. Disregarding the physical meaning, we can tune any constants to achieve a much higher accurate dip angle (Zhu et al., 2008). Thus, we extend the optimized coefficients from two to three for the second-order FD method and from four to six for the fourth-order FD method. Besides, we further relax the constant coefficient of the time-delay term (i.e., equation 6) by adding a very small perturbation. That is, there are four constant coefficients ready to be optimized in our scheme for the second-order FD method rather than the usual two coefficients, and there are seven constant coefficients for the fourth-order FD method rather than the usual four. Hence, the approximated dispersion relation in equation 5 finally becomes

$$\bar{k}_z = \frac{\omega}{v} \left(1 + f - \frac{a_1 \lambda u^2}{1 - (b_1 \eta + c_1 \lambda) u^2} - \frac{a_2 \lambda u^2}{1 - (b_2 \eta + c_2 \lambda) u^2} \right), \quad (13)$$

where f , a_1 , b_1 , c_1 , a_2 , b_2 , and c_2 are the constant coefficients ready to be optimized. This approximated dispersion relation degenerates to that of the second-order FD method if we set $a_2 = 0$. Table 1 shows the original coefficients using the Taylor-series expansion as well as the global optimization scheme. We will show later that the Taylor-series expansion provides us a solid basis for optimization; meanwhile, the extended number of coefficients and the relaxed coefficient greatly improve the flexibility to match the dispersion relation and significantly enhance the maximum accurate angle.

The error threshold of an optimization is usually set to be 1%. However, our numerical experiments show that the error threshold of 1% is only valid for a small-scale model (e.g., no deeper than 5 km). To obtain a much higher imaging accuracy, especially for deep-buried structures no matter whether they are low dips or steep

dips, we must employ a much smaller error threshold. On the other hand, we will lose the optimization freedom if the threshold is too tight. As a trade-off, we select the error threshold to be 0.5%, which is only half of the traditionally used 1%. In addition, we set the relaxed factor f in equation 13 to be no bigger than 0.1% because our experiments show that the improvements for wide angles are limited if we use $f \equiv 0$ as in traditional optimization schemes. Introducing the relaxed factor f will cause the zero-angle reflectors to be located at wrong depth positions; however, the error is negligible as shown in Figure 7. Theoretically, the maximum error is only several meters at a 10-km depth away from the earth's surface; thus f is feasible for the purpose of high-accuracy imaging. These settings of the error threshold and the relaxed factor greatly improve the imaging results for deep-buried structures. As a rule of thumb, these settings are valid for depth migration within a 10-km radius.

COMPARISON TO TRADITIONAL OPTIMIZATIONS

The dispersion relation of VTI media is more complex than that of isotropic media. As a result, it is difficult to design implicit FD schemes for wavefield extrapolation in anisotropic media through the analytic Taylor-series expansion (Shan, 2009). Therefore, Shan (2009) only shows a second-order FD method using the analytic Taylor-series expansion. To obtain a fourth-order FD scheme, he guesses a general form of the solution as follows (i.e., equation 20 in Shan, 2009)

$$k_z \approx \bar{k}'_z = \frac{\omega}{v} \left(1 - \frac{\alpha'_1 u^2}{1 - \beta'_1 u^2} - \frac{\alpha'_2 u^2}{1 - \beta'_2 u^2} - \dots \right); \quad (14)$$

then, he optimizes the constants α'_1 , β'_1 , α'_2 , and β'_2 by matching the dispersion relation. This is a practical way to design high-order FD schemes when the exact expression of the analytic Taylor-series expansion is difficult to obtain. The main difference between equations 5, 13, and 14 is that the coefficients of u^2 have different forms. Equation 14 tries the best to compress the FD operator because anisotropy parameters are invisible. Compared with equation 5, we see that the anisotropy parameters and the constant coefficients are actually combined into some newly defined constants. On the contrary, equation 13 tries the best to free and extend all possible constant coefficients besides remaining the explicit expression of anisotropy parameters.

Like other local optimization schemes (Ristow, 1999; Liu and Zhang, 2006), however, Shan's method also produces optimized

Table 1. Coefficients of implicit FD method using the analytic Taylor-series expansion and using the global optimization scheme (indicated by *).

Order	f	a_i	b_i	c_i
2nd	0.0	$a_1 = 0.5$	$b_1 = 1.0$	$c_1 = 0.25$
2nd*	-0.00099915	$a_1 = 0.46258453$	$b_1 = 1.00002193$	$c_1 = 0.40961897$
4th	0.0	$a_1 = 0.36180340$ $a_2 = 0.13819660$	$b_1 = 1.0$ $b_2 = 1.0$	$c_1 = 0.09549150$ $c_2 = 0.65450850$
4th*	-0.00070149	$a_1 = 0.46635550$ $a_2 = 0.02808554$	$b_1 = 1.00007105$ $b_2 = 0.99996132$	$c_1 = 0.25608018$ $c_2 = 0.90514874$

coefficients for each pair of ϵ and δ independently; thus, the accurate dip angle strongly depends on the parameters ϵ and δ . Theoretically, each group of optimized coefficients is only valid for the pair of ϵ and δ that are used to generate the optimized coefficients. Consequently, we could not guarantee the validity of a group of optimized coefficients for other pairs of ϵ and δ , especially in the presence of strong lateral variations in anisotropy. In addition, a large table is required to store the optimized coefficients, and a table lookup is needed during wavefield extrapolations. For strong anisotropy parameters, the number of optimized coefficients stored in the table is even up to several million, assuming that the sampling interval of the anisotropy parameters is of 0.001. Unfortunately, this interval is still not small enough for local optimization schemes to obtain an unconditionally safe table, as illustrated by Figure 1.

Figure 1 shows three groups of curves corresponding to the analytic Taylor-series expansion (i.e., equation 5), the locally optimized FD method using the least-squares approach (i.e., equation 14) and the globally optimized FD method using the simulated annealing algorithm (i.e., equation 13), respectively. We examine the robustness (or sensitivity) of their accuracy by introducing some small variations in anisotropy parameters. For each method, we plot nine curves around a typical group of anisotropy parameters with a uniform interval of 0.001. Figure 1a is around $\epsilon = 0.4$ and $\delta = 0.2$, and Figure 1b is around $\epsilon = 0.2$ and $\delta = -0.2$. For simplicity, only the fourth-order methods are discussed here. It is obvious that the FD method using the analytic Taylor-series expansion is always accurate within a 45° phase angle. Meanwhile, its accuracy is very stable for small variations in anisotropy parameters because the nine curves almost share the same position. In addition, the local optimization scheme using the least-squares approach and the global optimization scheme using the simulated annealing algorithm have much higher accurate phase angles than the analytic Taylor-series expansion.

However, the local optimization scheme based on equation 14 using a 1% error threshold (Shan, 2009) shows great diverging oscillation; that is, its curves exhibit significant error when they are corresponding to the surrounding rather than the central anisotropy parameters. Some curves even rush out of the error threshold of 1% at a 63° phase angle, which means that the local optimization scheme is virtually useless because it is close to the unoptimized result. This indicates that the local optimization scheme based on equation 14 is too sensitive to a small variation of anisotropy parameters. Although we can further reduce the grid interval to improve the reliability of this method, such as using 0.0005, the computational cost of generating the table and the table lookup would encounter great challenge because the number of the grid nodes over a strongly anisotropic region is probably more than tens of millions.

In contrast, the global optimization scheme based on equation 13 using a 0.5% error threshold behaves much better because all curves assemble closely within the error threshold. This allows us to use a much larger grid interval during the optimization, which helps to save the computational cost of generating the optimized coefficients. The maximum accurate phase angle is slightly smaller (at about 5°) than that of the local optimization scheme based on equation 14 using the least-squares approach. However, the former is much better than the latter because the former's error is within 0.5% rather than the latter's 1%. Therefore, we see that equation 13 using the simulated annealing algorithm provides us coefficients

with much better accuracy, robustness, and a much smaller error threshold than equation 14 using the least-squares approach does.

RELATIVE ERROR ANALYSES

We reproduce the scattering graph of ϵ and δ using the table in Thomsen (1986), as shown in Figure 2. Thomsen's table includes virtually all published data on measured anisotropy of sedimentary rocks, so we can use it to examine the capability of our optimized coefficients in handling practical anisotropic migration. We classify the anisotropy into three classes: weak anisotropy for $\epsilon \in [-0.03, 0.3]$ and $\delta \in [-0.1, 0.2]$ (see the shadow zone in Figure 2), strong anisotropy for $\epsilon \in [-0.1, 0.4]$ and $\delta \in [-0.3, 0.6]$ (see the gray zone in Figure 2), and extreme anisotropy for $\epsilon \in [-0.4, 0.8]$ and $\delta \in [-0.2, 1.22]$ (see the whole zone of Figure 2). Obviously, the weak anisotropy covers the densest area of anisotropy distributions, thus it would be the lowest level for a migration method to handle. The strong anisotropy covers almost the whole area of anisotropy distributions except one abrupt point of δ and four ultra points of ϵ , thus it would be the most practical level for a migration method to handle. The extreme anisotropy covers all anisotropy distributions and even beyond them to some extent, thus it would be the most severe case for a migration method to handle. We would seldom encounter the extreme anisotropy, but as a means of examination we still include it in our error analyses. A fine grid is set up over $\epsilon \in [\epsilon_{\min}, \epsilon_{\max}]$ and $\delta \in [\delta_{\min}, \delta_{\max}]$ with a uniform interval of 0.02. We also test on much denser grid to check on the reliability of relative error analyses, but we do not find sampling affect and gain the same conclusion. We plot all error curves on each grid nodes together to analyze the overall accuracy improvement due to the optimized coefficients.

Figures 3, 4, and 5 show the relative error versus phase angle for the weak, strong, and extreme anisotropy, respectively. We see that the error curves of the Taylor-series expanded and globally

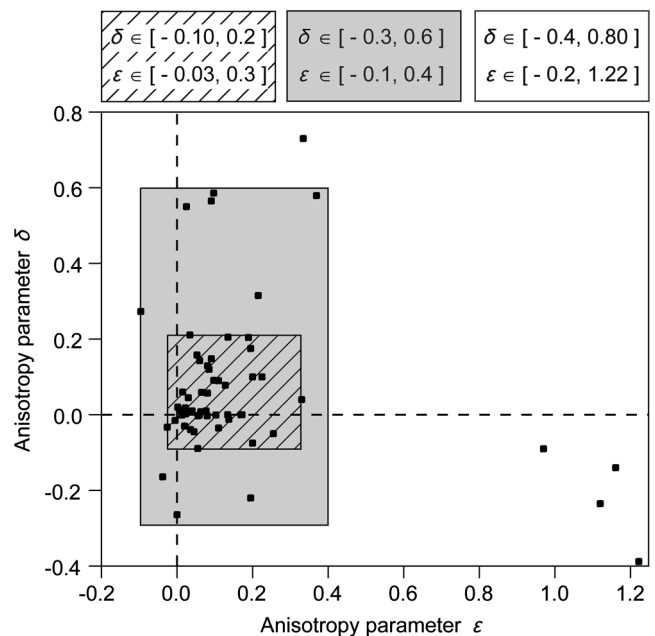


Figure 2. Scattering graph of Thomsen parameters of measured anisotropy in sedimentary rocks. This figure is produced according to the Table 1 of Thomsen (1986).

optimized FD methods are bundled, respectively. The error curves of the Taylor-series expanded FD method grow rapidly at a relatively low angle; in contrast, the error curves of the globally optimized FD method vibrate several times within the error threshold and finally rush out at a high angle. This means the globally optimized coefficients are effective in achieving a much higher accurate angle, given a tolerable threshold, no matter whether for weak, strong, or even extreme anisotropy.

The accurate phase angle decreases when the anisotropy becomes stronger. However, the improvement due to using the global optimization scheme is stable and always about 18°–22° for the second-order FD method and about 22°–27° for the fourth-order FD method. The improvements of the accurate angle due to using our global optimization scheme are shown in Figure 6 for various cases shown in Figures 3, 4, and 5. For the weak anisotropy (see Figure 3), the

accurate angle of the globally optimized second-order FD method is up to 60° from the original 41°, and that of the globally optimized fourth-order FD method is up to 78° from the original 56°. For the strong anisotropy (see Figure 4), the accurate angle of the globally optimized second-order FD method is up to 58° from the original 36°, and that of the globally optimized fourth-order FD method is up to 77° from the original 53°. Even for the extreme anisotropy (see Figure 5), the accurate angle of the globally optimized second-order FD method is still up to 50° from the original 32°, and that of the globally optimized fourth-order FD method is still up to 72° from the original 45°.

Note that only one group of optimized coefficients is given either for the second-order or for the fourth-order FD method, and all error curves and analyses are based on these two fixed groups of optimized coefficients shown in Table 1. This indicates that our optimized coefficients are global and no table is needed at all. In addition, our optimized coefficients show high accuracy under 0.5% error for all pairs of ϵ and δ on a fine grid; thus, we can guarantee the validity of our optimized coefficients for other pairs of ϵ and δ , especially in the presence of strong variations in anisotropy.

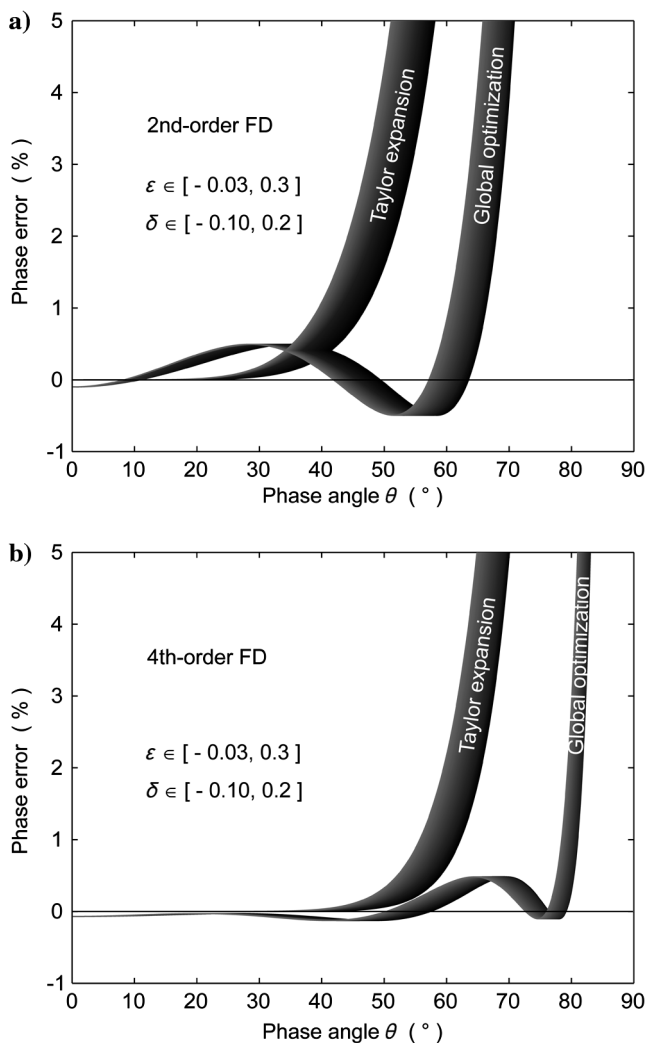


Figure 3. Relative error versus phase angle for weak anisotropy: (a) the second-order FD method, (b) the fourth-order FD method. A fine grid is set up over the ranges of anisotropy parameters in square brackets with a uniform interval of 0.02. Each group of Thomsen parameters produces a line for the Taylor-series expanded FD method and a line for the globally optimized FD method, respectively, using different gray scale. Figures 4 and 5 share the same color scale.

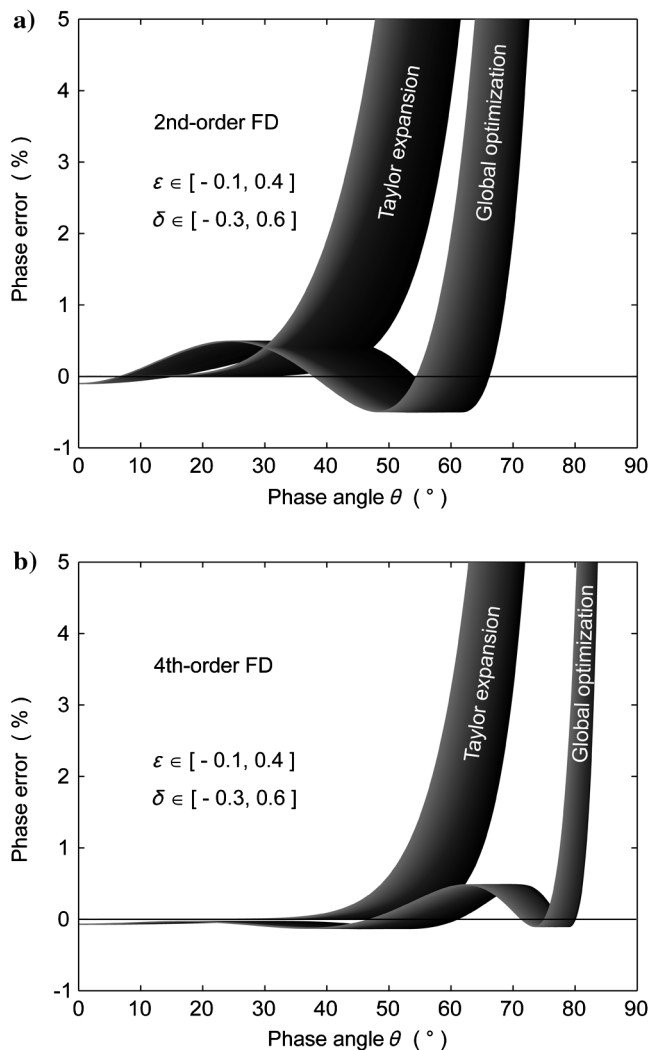


Figure 4. Relative error versus phase angle for strong anisotropy: (a) the second-order FD method, (b) the fourth-order FD method. See Figure 3 for a detailed description.

IMPULSE RESPONSES

In this section, we illustrate the relative error analyses by impulse responses. A 2D homogeneous medium is defined on a grid of 2000×600 with a grid spacing of 5 m. The vertical velocity of the q P-wave is $v = 4500$ m/s. A single input trace is located at the center of the upper surface. The traveltime is 600 ms with 2 ms sampling. The dominant frequency of a Ricker wavelet is 30 Hz.

Figure 7a and 7b shows vertical slices of the second-order and the fourth-order FD methods, respectively. This figure is generated using $\epsilon = 0.4$ and $\delta = 0.6$ (i.e., S4 in Figure 8), which are at one of the outer corners of strong anisotropy region. Each subfigure contains two parts: the left and right parts are the Taylor-series expanded and globally optimized ones, respectively. Obviously, the globally optimized FD methods show much wider ranges of accurate phase angle compared with the Taylor-series expanded ones. Figure 7 indicates that the improvement after using our global

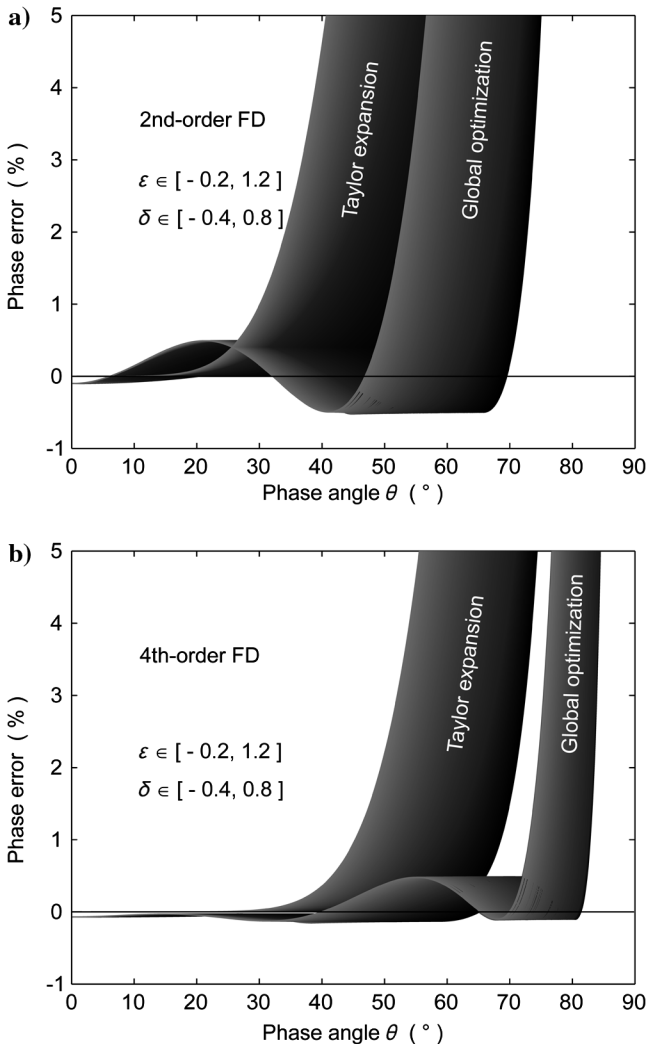


Figure 5. Relative error versus phase angle for extreme anisotropy: (a) the second-order FD method, (b) the fourth-order FD method. See Figure 3 for a detailed description.

optimization scheme is significant either for the second-order or for the fourth-order FD method.

Figure 8 shows some typical groups of anisotropy parameters. These groups are mainly on the outer corners of weak, strong and extreme anisotropy areas defined in Figure 2. Figures 9, 10, and 11 show the impulse responses of the globally optimized fourth-order FD method for weak, strong and extreme cases, respectively. We can see that all images show great agreements to the

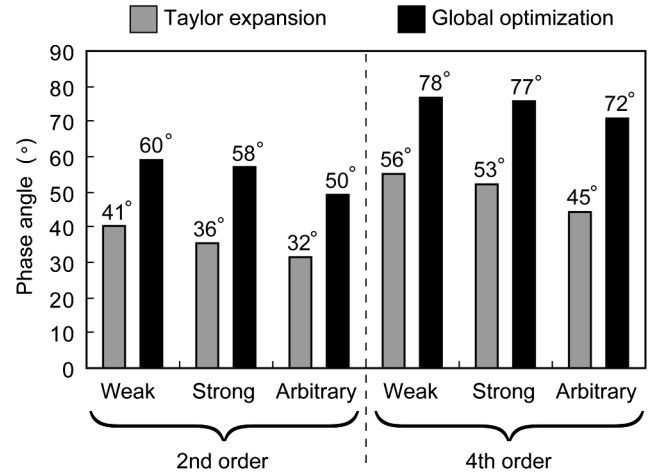


Figure 6. The improvement of accurate phase angle due to using our global optimization scheme for various cases shown in Figures 3, 4, and 5. The left and right part is about the second-order and fourth-order method, respectively. The gray bars denote the Taylor-series expanded FD method, and the dark bars denote the globally optimized FD method.

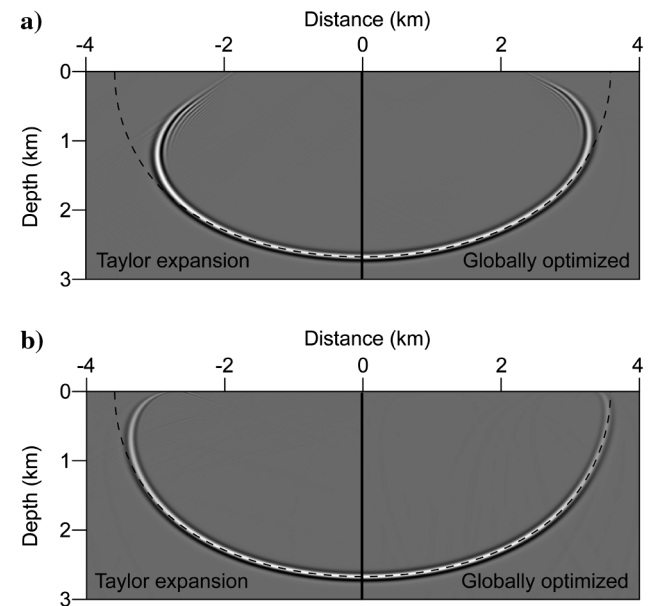


Figure 7. Impulse responses before and after using the global optimization scheme. This figure is generated by $\epsilon = 0.4$ and $\delta = 0.6$. (a) The second-order FD method. (b) The fourth-order FD method. Each subfigure contains two parts: the left and right parts are Taylor-series expanded and globally optimized FD methods, respectively.

theoretical positions (indicated by dashed curves), except for the high phase angles in the case of extreme anisotropy. This means our globally optimized FD method is able to image steep dips for most of the practical VTI media.

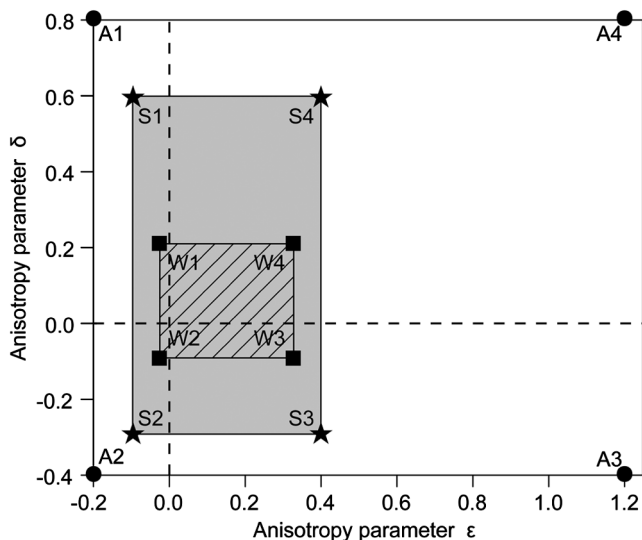


Figure 8. Some typical groups of anisotropy parameters used in Figures 9, 10, and 11. These groups are at the corners of weak, strong and extreme anisotropy areas defined in Figure 2, respectively. Four rectangles indicated by W denote weak anisotropy, four pentagrams indicated by S denote strong anisotropy, and four circles indicated by A denote extreme anisotropy.

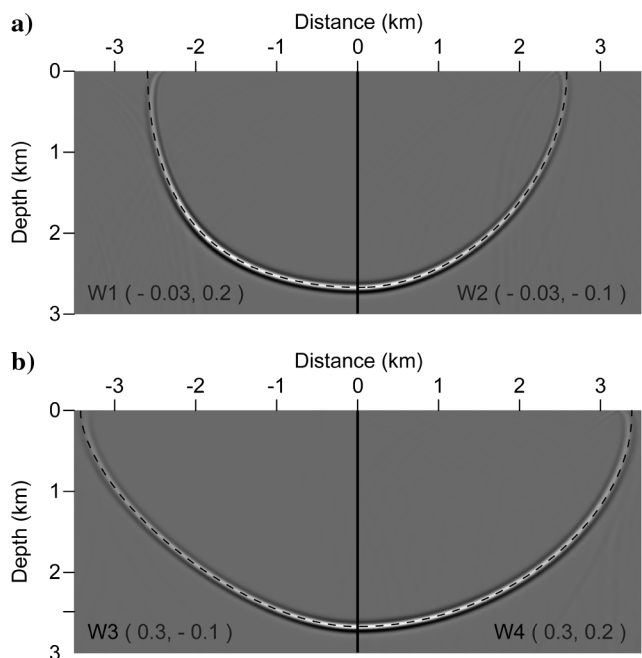


Figure 9. Impulse responses of the globally optimized fourth-order FD method for weak anisotropy. Each subfigure contains two parts, and each part is generated by different anisotropy parameters (i.e., W1–W4 shown in Figure 8). The dashed semicircle indicates the theoretical positions.

TEST ON STRONGLY VTI MODEL

To verify the capabilities of our globally optimized FD method, we test on a magnified Hess model, as shown in Figure 12. The Thomsen anisotropy parameters ϵ and δ are twice and four times as big as the original values, respectively. The grid is 2048×750 with a uniform spatial interval of 40 ft. A

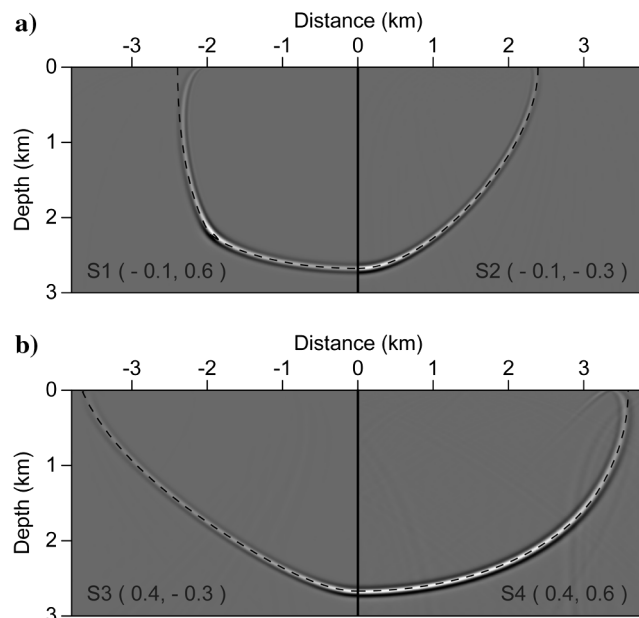


Figure 10. Impulse responses of the globally optimized fourth-order FD method for strong anisotropy. Each subfigure contains two parts, and each part is generated by different anisotropy parameters (i.e., S1–S4 shown in Figure 8). The dashed semicircle indicates the theoretical positions.

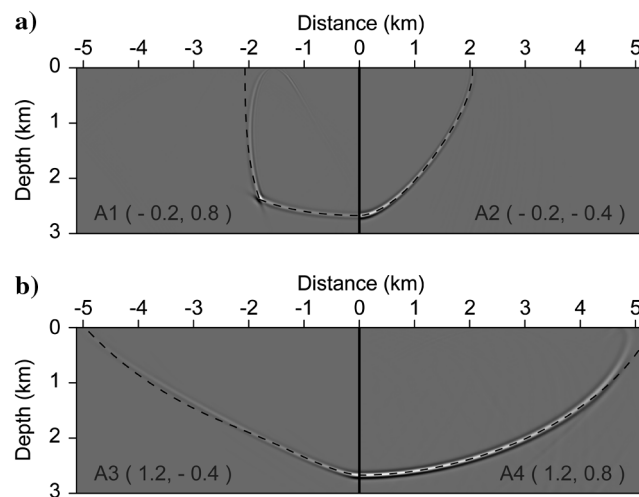


Figure 11. Impulse responses of the globally optimized fourth-order FD method for extreme anisotropy. Each subfigure contains two parts, and each part is generated by different anisotropy parameters (i.e., A1–A4 shown in Figure 8). The dashed semicircle indicates the theoretical positions.

two-way method (Alkhalifah, 2000; Zhang et al., 2005a) is used to generate 500 shot gathers. The dominant frequency of the Ricker wavelet is 15 Hz.

Figures 13 and 14 show the prestack depth migration results of the second-order and the fourth-order FD methods, respectively. We see that the accuracy is almost the same for each method at gentle structures. The difference is mainly at the dipping structures indicated by white arrows and an ellipse. The second-order FD method using the Taylor-series expansion has the lowest accuracy. After using our globally optimized coefficients, the second-order FD method is much more accurate, and the resulting accuracy is close to that of the fourth-order FD method using the Taylor-series expansion (compare Figures 13b and 14a). The globally optimized fourth-order FD method has the highest accuracy because it can perfectly image almost all structures, including low-velocity thin sediment targets under the salt body and salt flanks with steep dips. This indicates that our globally optimized FD methods are much better than the original ones based on the Taylor-series expansion. Therefore, we should use the globally optimized second-order method if the computational cost is serious and the wide-angle accuracy is not so important; beside, we should always use the globally optimized fourth-order FD method.

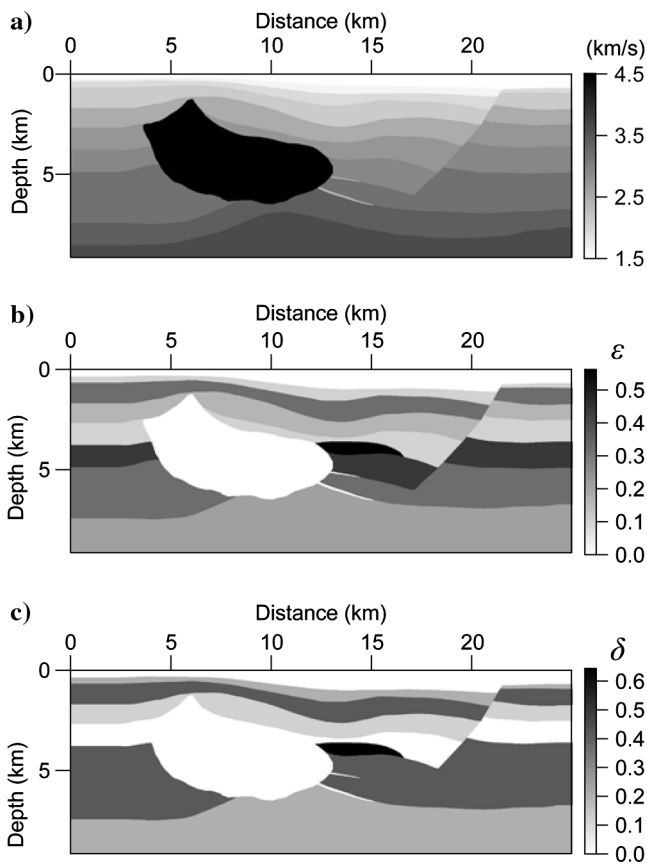


Figure 12. Strong anisotropy Hess model: (a) vertical velocity of the qP -wave, (b) anisotropy parameter $\varepsilon \in [0, 0.57]$, (c) anisotropy parameter $\delta \in [0, 0.63]$. This model is modified from the Hess model: the anisotropy parameters ε and δ are twice and four times as big as the original values, respectively.

DISCUSSION

The Fourier FD method (Ristow and Rühl, 1994) is very popular in imaging complex isotropic media. However its extension to the VTI media is much harder than that of the implicit FD method because it is difficult to select proper references of anisotropy parameters (Hua et al., 2006; Shan, 2009). If we select the reference anisotropy parameters as the minimum of each layer, we will encounter a huge table because we have to list each possible case and optimize the coefficients independently. If we set the reference anisotropy parameters to be zero for each layer, we will get a simplified table (Shan, 2009); but will also lose too much accuracy because the reference is too far away from the real value. This problem will be very serious especially when the anisotropy is strong, or when the variation of the anisotropy is strong. Therefore, we only perform optimization on the implicit FD method in the text. The global optimization scheme for the Fourier FD is still open.

Using the global optimization scheme over the low-accuracy subregions sounds helpful for improving the maximum phase angle. Thus, we try our global optimization scheme separately on each block of a 5×5 massive partition of anisotropy parameters. However, only a slight improvement at about 3° is obtained for big δ regions and almost no improvement is obtained for the other

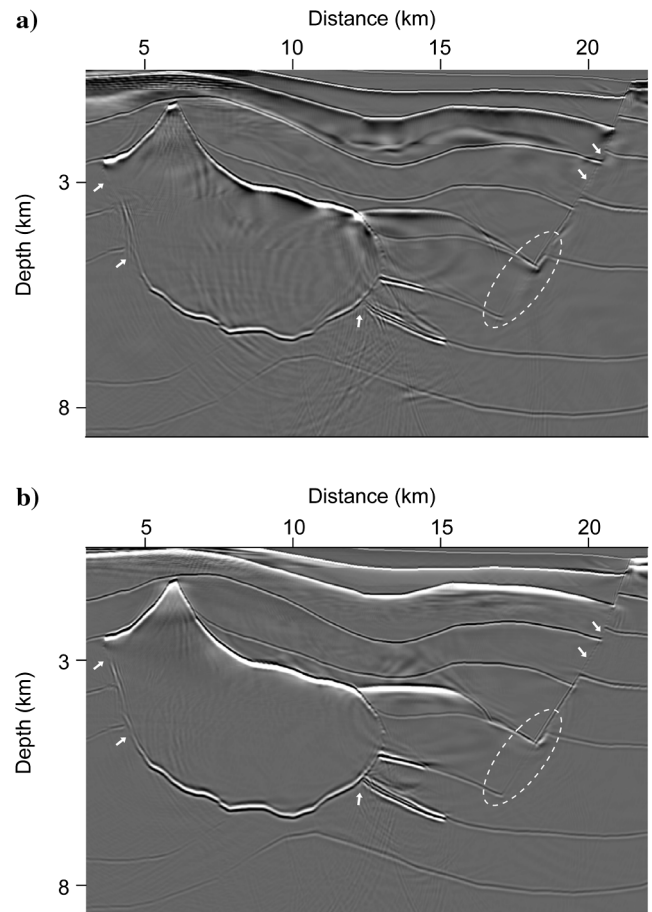


Figure 13. Comparison between migration results obtained by the second-order implicit FD method: (a) using the analytic Taylor-series expansion, (b) using the global optimization scheme.

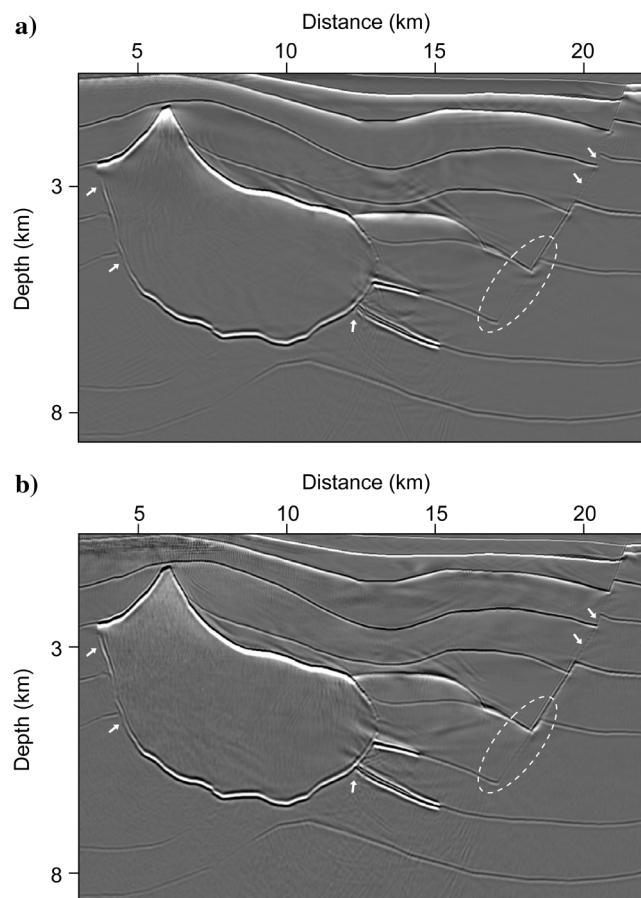


Figure 14. Comparison between migration results obtained by the fourth-order implicit FD method: (a) using the analytic Taylor-series expansion, (b) using the global optimization scheme.

regions. Maybe a much smaller massive partition is feasible at the cost of a much larger table.

The dispersion relation for acoustic VTI media is obtained by setting the qS -wave velocity to be zero, which is valid only when the anisotropy is not so strong. However, the critical condition of this approximation has not been clear until now. Consequently, we suggest using our globally optimized coefficients only when the anisotropy is not so strong. Our globally optimized coefficients can be used for 3D cases and the compensations of two-way splitting error (e.g., Li, 1991; Wang, 2001; Fei and Etgen, 2002; Bakker, 2009; Zhang, 2009; Zhang and Yao, 2011).

CONCLUSIONS

We present an implicit FD method using the analytic Taylor-series expansion for imaging strongly VTI media. The accuracy of the fourth-order FD method is always above 45° even for extreme Thomsen anisotropy parameters in realities. To improve the wide-angle accuracy, we describe a global optimization scheme using the simulated annealing algorithm. We first extend the total number of constant coefficients and then relax the coefficient of the time-delay term to enhance the flexibility of optimization. This global optimization scheme optimizes the constant coefficients on a fine grid over a wide range of Thomsen anisotropy parameters. The resulting optimized coefficients satisfy the objective function

on all grid nodes simultaneously. The analytic Taylor-series expansion provides us a solid basis for optimization, and the extended number of constant coefficients, as well as the relaxed coefficient, provide great flexibility when matching the dispersion relation; otherwise, the simulated annealing algorithm plays an important role in successfully searching the maximum accurate phase angle. The error threshold is set to be only 0.5%; in addition, the relative error within 0° – 50° phase angles is only about 0.1% for the globally optimized fourth-order FD method. These greatly reduced errors provide much higher accuracy for imaging much deeper subsurfaces, especially for large models.

Compared with traditional local optimization, our global optimization scheme does not need a table. Only one group of optimized coefficients is required for each order of the FD method. In addition, the global optimization scheme can guarantee the accuracy in the presence of strong anisotropy as well as strong variations in anisotropy parameters. The globally optimized FD method is accurate to about 60° for the second-order method and to about 80° for the fourth-order method. The accurate dip angle is about 20° larger than that of the unoptimized method for most practical VTI media, including weak, strong, and even extreme cases. Therefore, the globally optimized FD methods are ideal for imaging strongly VTI media.

ACKNOWLEDGMENTS

We thank Amerada Hess for providing the VTI model. We also thank Bialong Hua for helpful discussions. We are grateful to Yaxun Tang and anonymous reviewers for their valuable comments and suggestions. We are heartily grateful to editor Tamas Nemeth for encouraging us to rewrite the manuscript and providing many constructive suggestions. This research was supported by the National Natural Science Foundation of China (Grant No. 41074092), the Major State Basic Research Development Program of China (973 Program) (Grant No. 2009CB219404), and the National Major Project of China (Grant No. 2011ZX05008-006).

REFERENCES

- Alkhalifah, T., 1998, Acoustic approximations for processing in transversely isotropic media: *Geophysics*, **63**, 623–631, doi: [10.1190/1.1444361](https://doi.org/10.1190/1.1444361).
- Alkhalifah, T., 2000, An acoustic wave equation for anisotropic media: *Geophysics*, **65**, 1239–1250, doi: [10.1190/1.1444815](https://doi.org/10.1190/1.1444815).
- Amazonas, D., R. Aleixo, J. Schleicher, and J. C. Costa, 2010, Anisotropic complex Padé hybrid finite-difference depth migration: *Geophysics*, **75**, no. 2, S51–S59, doi: [10.1190/1.3337317](https://doi.org/10.1190/1.3337317).
- Bakker, P. M., 2009, A stable one-way wave propagator for VTI media: *Geophysics*, **74**, no. 5, WB3–WB17, doi: [10.1190/1.3196818](https://doi.org/10.1190/1.3196818).
- Claerbout, J. F., 1985, *Imaging the earth's interior*: Blackwell Scientific Publications, Inc.
- Etgen, J., 1994, Stability of explicit depth extrapolation through laterally varying media: 64th Annual International Meeting, SEG, Expanded Abstracts, 1266–1269.
- Etgen, J., S. H. Gray, and Y. Zhang, 2009, An overview of depth imaging in exploration geophysics: *Geophysics*, **74**, no. 6, WCA5–WCA17, doi: [10.1190/1.3223188](https://doi.org/10.1190/1.3223188).
- Fei, T. W., and J. T. Etgen, 2002, Domain decomposition for 3-D finite-difference depth extrapolation: 72nd Annual International Meeting, SEG, Expanded Abstracts, 1160–1163.
- Fei, T. W., and C. L. Liner, 2008, Hybrid Fourier finite-difference 3D depth migration for anisotropic media: *Geophysics*, **73**, no. 2, S27–S34, doi: [10.1190/1.2828704](https://doi.org/10.1190/1.2828704).
- Ferguson, R. J., and G. F. Margrave, 2002, Depth imaging in anisotropic media by symmetric non-stationary phase shift: *Geophysical Prospecting*, **50**, 281–288, doi: [10.1046/j.1365-2478.2002.00318.x](https://doi.org/10.1046/j.1365-2478.2002.00318.x).
- Han, Q., and R. S. Wu, 2005, A one-way dual-domain propagator for scalar qP -waves in VTI media: *Geophysics*, **70**, no. 2, D9–D17, doi: [10.1190/1.1884826](https://doi.org/10.1190/1.1884826).

- Hua, B. L., H. Calandra, and P. Williamson, 2006, 3D common azimuth Fourier finite-difference depth migration in transversely isotropic media: 76th Annual International Meeting, SEG, Expanded Abstracts, 2387–2391.
- Huang, L. J., and M. C. Fehler, 2000, Globally optimized Fourier finite-difference migration method: 70th Annual International Meeting, SEG, Expanded Abstracts, 802–805.
- Kirkpatrick, S., C. D. Gelatt, and M. P. Vecchi, 1983, Optimization by simulated annealing: *Science*, **220**, 671–680, doi: [10.1126/science.220.4598.671](https://doi.org/10.1126/science.220.4598.671).
- Larner, K., and J. K. Cohen, 1993, Migration error in transversely isotropic media with linear velocity variation in depth: *Geophysics*, **58**, 1454–1467, doi: [10.1190/1.1443360](https://doi.org/10.1190/1.1443360).
- Lee, M., and S. Suh, 1985, Optimization of one-way wave equations: *Geophysics*, **50**, 1634–1637, doi: [10.1190/1.1441853](https://doi.org/10.1190/1.1441853).
- Le Rousseau, J. H., 1997, Depth migration in heterogeneous, transversely isotropic media with the phase-shift-plus-interpolation method: 67th Annual International Meeting, SEG, Expanded Abstracts, 1703–1706.
- Le Rousseau, J. H., and M. V. de Hoop, 2001, Scalar generalized-screen algorithms in transversely isotropic media with a vertical symmetry axis: *Geophysics*, **66**, 1538–1550, doi: [10.1190/1.1487100](https://doi.org/10.1190/1.1487100).
- Li, Z., 1991, Compensating finite-difference errors in 3D migration and modeling: *Geophysics*, **56**, 1650–1660, doi: [10.1190/1.1442975](https://doi.org/10.1190/1.1442975).
- Liu, L., and J. Zhang, 2006, Optimum split-step Fourier one-way operators for seismic modeling and imaging in 3D VTI media: *Geophysical Research Letters*, **33**, L09308, doi: [10.1029/2006GL025849](https://doi.org/10.1029/2006GL025849).
- Ma, Z., 1982, Steep dip finite difference migration: *Oil Geophysical Prospecting (in Chinese)*, **1**, 6–15.
- Meadows, M. A., and W. L. Abriell, 1994, 3-D poststack phase-shift migration in transversely isotropic media: 64th Annual International Meeting, SEG, Expanded Abstracts, 1205–1208.
- Pedersen, Ø., B. Ursin, and H. K. Helgesen, 2010, One-way wave-equation migration of compressional and converted waves in a VTI medium: *Geophysics*, **75**, no. 6, S237–S248, doi: [10.1190/1.3509466](https://doi.org/10.1190/1.3509466).
- Ren, J., C. Gerrard, J. McClean, and M. Orlovich, 2005, Prestack wave-equation depth migration in VTI media: *The Leading Edge*, **24**, 618–620, doi: [10.1190/1.1946218](https://doi.org/10.1190/1.1946218).
- Ristow, D., 1999, Migration of transversely isotropic media using implicit finite-difference operators: *Journal of Seismic Exploration*, **8**, 39–55.
- Ristow, D., and T. Rühl, 1994, Fourier finite-difference migration: *Geophysics*, **59**, 1882–1893, doi: [10.1190/1.1443575](https://doi.org/10.1190/1.1443575).
- Sen, M. K., and P. L. Stoffa, 1991, Nonlinear one-dimensional seismic waveform inversion using simulated annealing: *Geophysics*, **56**, 1624–1638, doi: [10.1190/1.1442973](https://doi.org/10.1190/1.1442973).
- Shan, G., 2009, Optimized implicit finite-difference and Fourier finite-difference migration for VTI media: *Geophysics*, **74**, no. 6, WCA189–WCA197, doi: [10.1190/1.3202306](https://doi.org/10.1190/1.3202306).
- Thomsen, L., 1986, Weak elastic anisotropy: *Geophysics*, **51**, 1954–1966, doi: [10.1190/1.1442051](https://doi.org/10.1190/1.1442051).
- Thorbecke, J. W., K. Wapenaar, and G. Swinnen, 2004, Design of one-way wavefield extrapolation operators, using smooth functions in WLSQ optimization: *Geophysics*, **69**, 1037–1045, doi: [10.1190/1.1778246](https://doi.org/10.1190/1.1778246).
- Tsvankin, I., 1996, P-wave signatures and notation for transversely isotropic media: An overview: *Geophysics*, **61**, 467–483, doi: [10.1190/1.1443974](https://doi.org/10.1190/1.1443974).
- Uzcategui, O., 1995, 2-D depth migration in transversely isotropic media using explicit operators: *Geophysics*, **60**, 1819–1829, doi: [10.1190/1.1443914](https://doi.org/10.1190/1.1443914).
- Wang, Y., 2001, ADI plus interpolation: Accurate finite-difference solution to 3D paraxial wave equation: *Geophysical Prospecting*, **49**, 547–556, doi: [10.1046/j.1365-2478.2001.00278.x](https://doi.org/10.1046/j.1365-2478.2001.00278.x).
- Xie, X. B., and R. S. Wu, 1998, Improve the wide angle accuracy of screen method under large contrast: 68th Annual International Meeting, SEG, Expanded Abstracts, 1811–1814.
- Xie, X. B., and R. S. Wu, 1999, Improve the wide-angle accuracy of screen propagator for elastic wave propagation: 69th Annual International Meeting, SEG, Expanded Abstracts, 1863–1866.
- Zhang, J., D. J. Verschuur, and C. P. A. Wapenaar, 2001, Depth migration of shot records in heterogeneous transversely isotropic media using optimum explicit operators: *Geophysical Prospecting*, **49**, 287–299, doi: [10.1046/j.1365-2478.2001.00255.x](https://doi.org/10.1046/j.1365-2478.2001.00255.x).
- Zhang, J. H., W. M. Wang, S. Q. Wang, and Z. X. Yao, 2010, Optimized Chebyshev Fourier migration: A wide-angle dual-domain method for media with strong velocity contrasts: *Geophysics*, **75**, no. 2, S23–S34, doi: [10.1190/1.3350861](https://doi.org/10.1190/1.3350861).
- Zhang, J. H., and Z. X. Yao, 2011, Reducing two-way splitting error of FFD method in dual domains: *Geophysics*, **76**, no. 4, S165–S175, doi: [10.1190/1.3590214](https://doi.org/10.1190/1.3590214).
- Zhang, L., B. Hua, and H. Calandra, 2005a, 3D Fourier finite-difference anisotropic depth migration: 75th Annual International Meeting, SEG, Expanded Abstracts, 1914–1917.
- Zhang, L., J. W. Rector, and G. M. Hoversten, 2005b, Finite-difference modelling of wave propagation in acoustic tilted TI media: *Geophysical Prospecting*, **53**, 843–852, doi: [10.1111/gpr.2005.53.issue-6](https://doi.org/10.1111/gpr.2005.53.issue-6).
- Zhang, Y., 2009, Four-way splitting implicit finite-difference algorithm on rectangular grids and its application to VTI migration: *Geophysical Prospecting for Petroleum (in Chinese)*, **48**, 27–33.
- Zhang, Y., and H. Zhang, 2009, A stable TTI reverse time migration and its implementation: 79th Annual International Meeting, SEG, Expanded Abstracts, 2794–2798.
- Zhu, S. W., J. H. Zhang, and Z. X. Yao, 2008, Globally optimized Fourier finite-difference operator using simulated annealing algorithm based on multi-parameter: *Chinese Journal of Geophysics (in Chinese)*, **51**, 1844–1850.